AGU PUBLICATIONS

Geochemistry, Geophysics, Geosystems

RESEARCH ARTICLE
10.1002/2017GC006977

Key Points:
- Postcollisional magmatic activity in the Awulale Mountains, Tianshan Orogen, yields early Permian and Triassic ages
- The early Permian mantle transition was related to partial subduction of the Tarim continental crust beneath the Tianshan Orogen
- The second stage in the middle Triassic, there was a reversion to more asthenospheric sources, related to lithospheric thinning

Supporting Information:
- Supporting Information S1
- Table S1
- Table S2
- Table S3
- Table S4

Correspondence to:
G.-J. Tang,
tanggj@gig.ac.cn

Citation:
Tang, G.-J., Cawood, P. A., Wyman, D. A., Wang, Q., & Zhao, Z.-H. (2017). Evolving mantle sources in postcollisional early Permian-Triassic magmatic rocks in the heart of Tianshan Orogen (western china). *Geochemistry, Geophysics, Geosystems*, *18*. https://doi.org/10.1002/2017GC006977

Received 17 APR 2017
Accepted 17 OCT 2017
Accepted article online 25 OCT 2017

Evolving Mantle Sources in Postcollisional Early Permian-Triassic Magmatic Rocks in the Heart of Tianshan Orogen (Western China)

Gong-Jian Tang[1,2], Peter A. Cawood[3,4], Derek A. Wyman[5], Qiang Wang[1,2,6], and Zhen-Hua Zhao[7]

[1]State Key Laboratory of Isotope Geochemistry, Guangzhou Institute of Geochemistry, Chinese Academy of Sciences, Guangzhou, China, [2]CAS Center for Excellence in Tibetan Plateau Earth Sciences, Beijing, China, [3]School of Earth, Atmosphere and Environment, Monash University, Melbourne, Vic, Australia, [4]Department of Earth Sciences, University of St. Andrews, Fife, UK, [5]School of Geosciences, Division of Geology and Geophysics, University of Sydney, Sydney, NSW, Australia, [6]University of Chinese Academy of Sciences, Beijing, China, [7]Key laboratory of Mineralogy and Metallogeny, Guangzhou Institute of Geochemistry, Chinese Academy of Sciences, Guangzhou, China

Abstract Magmatism postdating the initiation of continental collision provides insight into the late stage evolution of orogenic belts including the composition of the contemporaneous underlying subcontinental mantle. The Awulale Mountains, in the heart of the Tianshan Orogen, display three types of postcollisional mafic magmatic rocks. (1) A medium to high K calc-alkaline mafic volcanic suite (~280 Ma), which display low La/Yb ratios (2.2–11.8) and a wide range of $\varepsilon_{Nd}(t)$ values from +1.9 to +7.4. This suite of rocks was derived from melting of depleted metasomatized asthenospheric mantle followed by upper crustal contamination. (2) Mafic shoshonitic basalts (~272 Ma), characterized by high La/Yb ratios (14.4–20.5) and more enriched isotope compositions ($\varepsilon_{Nd}(t) = +0.2 - +0.8$). These rocks are considered to have been generated by melting of lithospheric mantle enriched by melts from the Tarim continental crust that was subducted beneath the Tianshan during final collisional suturing. (3) Mafic dikes (~240 Ma), with geochemical and isotope compositions similiar to the ~280 Ma basaltic rocks. This succession of postcollision mafic rock types suggests there were two stages of magma generation involving the sampling of different mantle sources. The first stage, which occurred in the early Permian, involved a shift from depleted asthenospheric sources to enriched lithospheric mantle. It was most likely triggered by the subduction of Tarim continental crust and thickening of the Tianshan lithospheric mantle. During the second stage, in the middle Triassic, there was a reversion to more asthenospheric sources, related to postcollision lithospheric thinning.

1. Introduction

Orogenic magmatism can be grouped to two types based on its temporal relationship to the tectonic evolution of orogenic belts: subduction related and postcollisional (Martin & Piwinskii, 1972). Postcollisional mafic magmatism provides a unique opportunity to study the asthenospheric and lithospheric mantle after the cessation of arc magmatism, and is important in understanding the evolution of orogenic belts (Carlson et al., 2005). Calc-alkaline and potassium-enriched (K-rich) volcanic rocks are two types of postcollisional magmatism recognized in the modern mountain belts in Tibet (Guo et al., 2015a, 2015b, 2006; Turner et al., 1996; Williams et al., 2004) and the Turkish-Iranian Plateau (Allen et al., 2013; Neill et al., 2015). Postcollisional mafic rocks are generally considered to be derived by partial melting of enriched mantle sources (Kirchenbaur et al., 2012). However, there is no consensus on the nature of the metasomatic components that cause mantle enrichment, such as whether fluid or melt derived from either subducted oceanic (e.g., Lustrino et al., 2011; Prelević et al., 2010) or continental crust (e.g., Ding et al., 2003; Guo et al., 2013, 2015b; Mahéo et al., 2002; Zhao et al., 2009).

The Tianshan Orogen in central Asia records the closure of the Paleo-Asian Ocean associated with convergence between the southern active margin of the Siberian craton and the passive margin of the Tarim Craton (Xiao et al., 2013), although recent studies indicate that the northern Tarim has been active margin during the middle Paleozoic (e.g., Lin et al., 2013) (Figure 1). Postcollisional episodes of Permian and Triassic volcanism are inferred to have occurred within an overall extensional regime (Chen et al., 2015; Luo et al.,

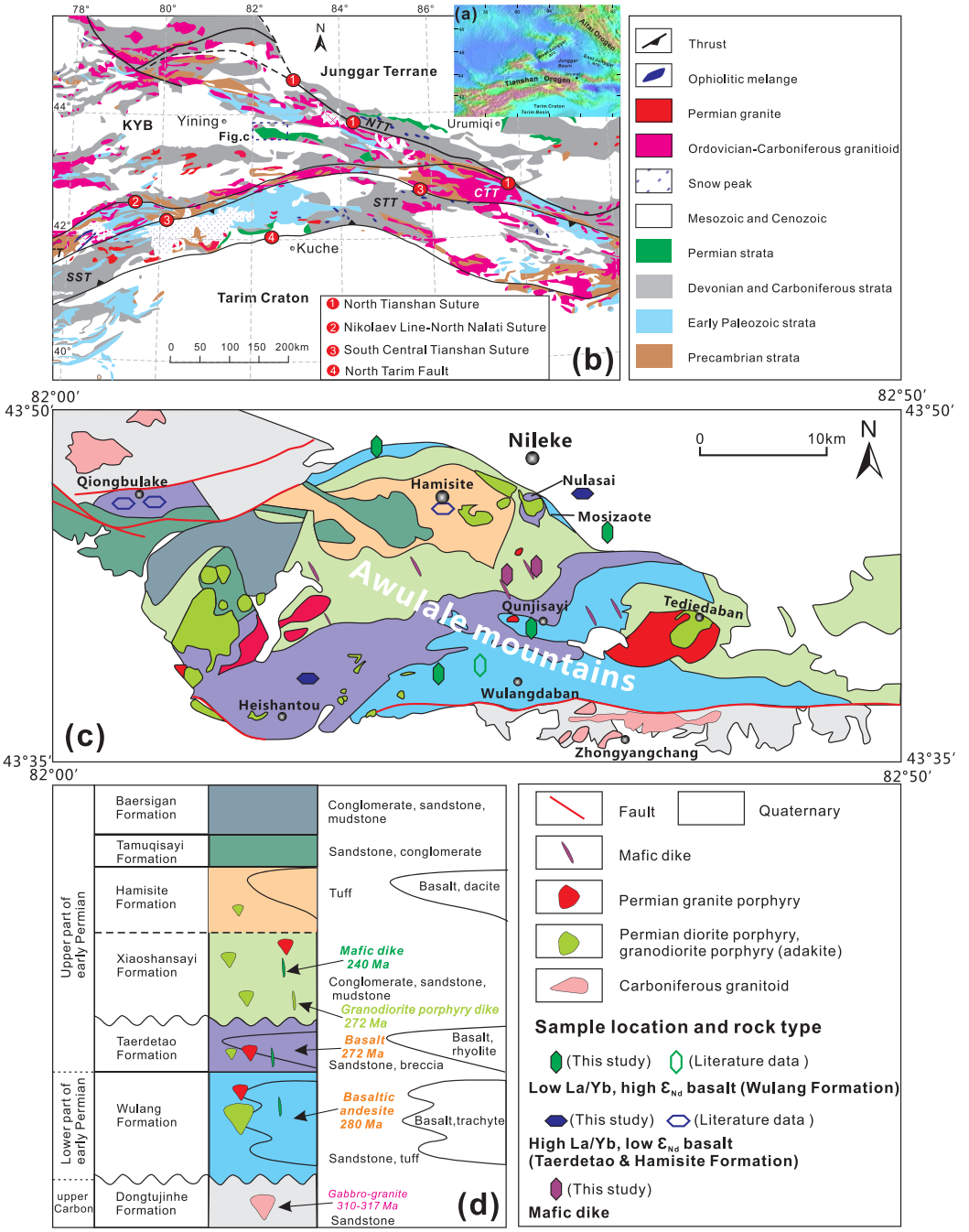

Figure 1. (a) Digital topography of North Xinjiang and adjact area of the sourhern Central Asian Orogenic Belt (original data from U.S. Geological Survey [http://eros.usgs.gov/products/elevation/gtopo30.html]) showing the Altai, Junggar, Tianshan Orogens and Tarim Craton from northeast to southwest. (b) Geological and tectonic sketch map of the Chinese Tianshan Orogen (modified after Gao et al., 2011; Xiao et al., 2013). (c) Geological map and (d) stratigraphic sequence of the western part of the Awulale Mountain. Sample locations and rock types are also shown. The magmatism ages are from Tang et al. (2017b), Tang et al. (2014), and this study.

2013; Ye et al., 2013) (Figure 1). Contemporaneous with the mafic volcanism in this region are abundant A-type granites and subordinate adakites, which are attributed to crustal melting as a result of enhanced heat input into the crust triggered by upwelling asthenosphere (Long et al., 2011; Tang et al., 2017b, 2010; Zhao et al., 2008). Most research into the tectonic evolution of the Tianshan Orogen has focused on the Paleozoic granitoids (Long et al., 2011; Tang et al., 2014, 2010). However, the mantle evolution processes of the Tianshan Orogen, postcollision, are poorly constrained. The geochemical and isotopic signatures of the

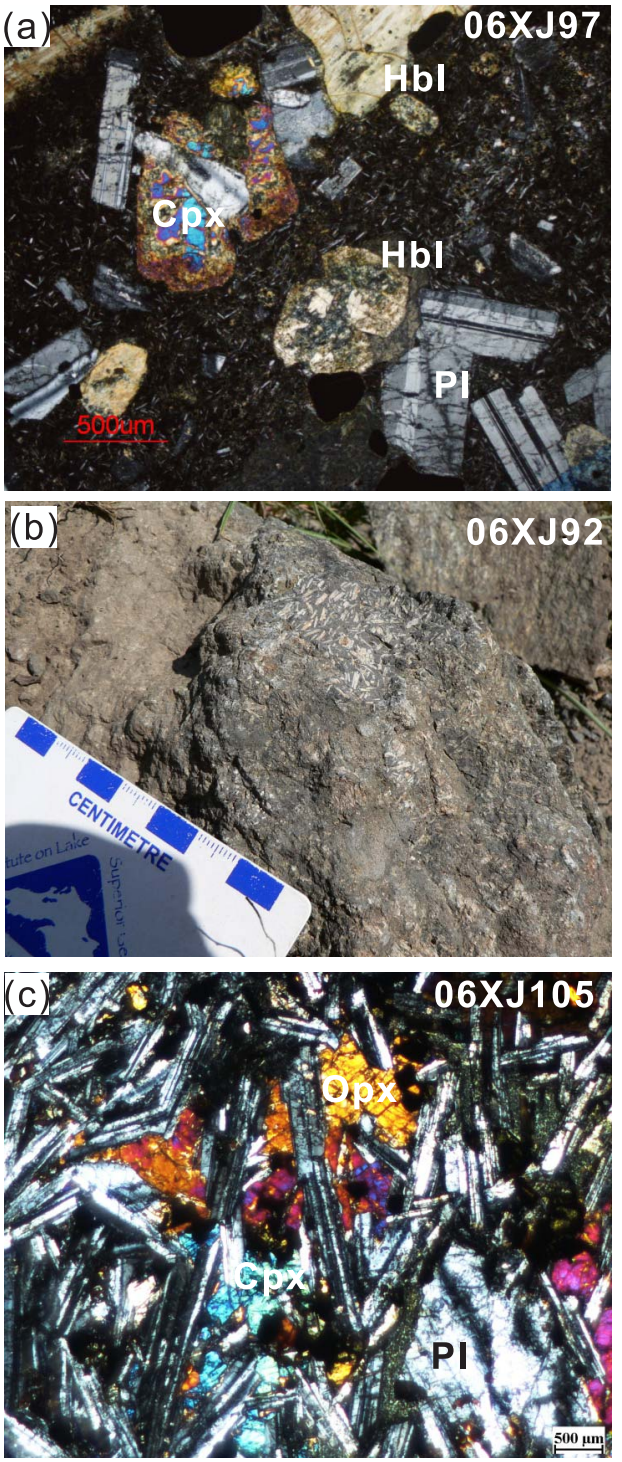

Figure 2. Photomicrographs showing the main textures and mineral assemblages in the magmatic rocks from the Awulale Mountains. (a) Early Permian lower group basaltic andesite; (b) early Permian upper group basaltic rock; (c) mafic dike. Cpx, clinopyroxene; Opx, orthopyroxene; Pl, plagioclase; Hbl, hornblende.

postcollisional mafic rocks of different ages in the same region have the potential to provide important insights into the evolution of mantle sources from which they are derived (Murphy & Dostal, 2007).

The Awulale Mountains, in the heart of the Tianshan Orogen, consist of early Permian volcanic rocks with Triassic mafic dikes (Figure 1) (Chen et al., 2015; Luo et al., 2013; Ye et al., 2013). Although these Permian volcanic rocks are well mapped and documented, most studies are confined to those of early Permian age from a limited region in the Awulale Mountains. In addition, there is a lack of precise age data for these volcanic rocks, limiting understanding of the chemical characteristics of mantle sources and the geodynamic processes involved. We integrate new age and geochemical (major element, trace element, and Sr-Nd isotopic) data with previous work (Chen et al., 2015; Luo et al., 2013; Ye et al., 2013) for the Permian-Triassic mafic rocks from the Awulale Mountains, to resolve their petrogenesis and to evaluate relationships between postcollisional magmatism and mantle sources within the evolving postcollisional framework of the Tianshan Orogen.

2. Geological Background and Petrology

The Tianshan Orogen is a major component of the southwestern Central Asian Orogenic Belt (CAOB) and extends more than 2,500 km from Uzbekistan to Xinjiang in China. The Xinjiang segment of the orogen is bounded by the Tarim Craton to the south and the Junggar terrane to the north (Figure 1). There is general agreement that final ocean closure associated with the termination of oceanic subduction, and collision between the Tarim Craton and Kazakhstan-Yili-Central Tianshan arc occurred at the end of the Carboniferous, and that during the early Permian the Tianshan Orogen lay in a postcollisional setting (Gao et al., 2011; Han et al., 2011; Seltmann et al., 2011), although it remains a controversial issue (Xiao et al., 2013). Postcollisional volcanic rocks are scattered spatially and temporally across the orogen (Figure 1) and, in addition, early Permian A-type granites are widespread (Konopelko et al., 2007; Seltmann et al., 2011; Tang et al., 2010).

The west-east trending Awulale Mountains comprise upper Carboniferous and lower Permian volcanic-sedimentary formations (Figure 1). The upper Carboniferous rock units are restricted to the southeast and northwest of the area and consist of basalt, andesite, tuff and sandstone. The Permian geology of the Awulale Mountains is dominated by two assemblages of spatially associated Permian volcanic rocks (Figure 1): (1) the lower part, present mainly in the southern and northeast parts of the Awulale Mountains, consists of early Permian lava flows and associated volcanic breccias of basalt, trachyte, rhyolite, along with interstratified sandstone and tuff. They uncomfortably overlie the Carboniferous succession. (2) The upper part of the early Permian units consists of conglomerate, sandstone, mudstone, basalt, and dacite, and is restricted to a small area in the northwest part of the Awulale Mountains. Minor, steeply dipping middle Triassic mafic dikes intrude into Permian volcanic-sedimentary formations and have a trend of 150° (Figure 1).

The lower group basalts and basaltic andesites exhibit porphyritic textures and mainly consist of plagioclase, clinopyroxene, amphibole, and Fe-Ti oxide phenocrysts, with similar microlitic minerals in the groundmass (Figure 2a). The upper group basalts are porphyritic with plagioclase and amphibole phenocrysts. The groundmass is composed of plagioclase, amphibole, chlorite, and basaltic

glass with minor pyroxene (Figure 2b). The middle Triassic mafic dikes are fine grained and consist of plagioclase, clinopyroxene, and orthopyroxene.

3. Analytical Methods

Zircons were separated using conventional heavy liquid and magnetic separation techniques. Cathodoluminescence (CL) images were obtained for zircons prior to analysis, using a JEOL JXA-8100 Superprobe at Guangzhou Institute of Geochemistry, Chinese Academy of Sciences (GIG-CAS), in order to characterize internal structures and choose potential target sites for U-Pb dating. LA-ICP-MS U-Pb zircon analyses were conducted on an Agilent 7500 ICP-MS equipped with a 193 nm laser and a beam diameter of ~30 μm, housed at the State Key Laboratory of Geological Processes and Mineral Resources, Faculty of Earth Sciences, China University of Geosciences (Wuhan). Zircon 91500 was used as the standard (Wiedenbeck et al., 1995) and the silicate glass standard NIST 610 was used to optimize operating parameters. The weighted mean U-Pb ages and Concordia plots were processed using an Isoplot/Ex v.3.0 program (Ludwig, 2003). Subsequently, Lu-Hf isotope measurements on the dated spots in each zircon grain were performed using a Neptune multicollector ICP-MS equipped with a Geolas-193 laser-ablation system at IGG-CAS (Wu et al., 2006).

After crushing, unweathered rock fractions were selected and subjected to ultrasonic cleaning in distilled water with $<5\%$ HNO_3, dried and handpicked to remove visible contamination, and then pulverized.

Major element oxides were determined by standard X-ray fluorescence (XRF) (Li et al., 2006). Trace elements were analyzed by inductively coupled plasma mass spectrometry (ICP-MS), using a Perkin-Elmer Sciex ELAN 6000 instrument at GIG-CAS (Li et al., 2006). Analytical precision for most elements is better than 3%.

Sr and Nd isotopic analyses were performed on a Micromass Isoprobe multicollector ICPMS at the GIG-CAS (Li et al., 2006). Sr and REE were separated using cation columns, and Nd fractions were further separated by HDEHP-coated Kef columns. Measured $^{87}Sr/^{86}Sr$ and $^{143}Nd/^{144}Nd$ ratios were normalized to $^{86}Sr/^{88}Sr = 0.1194$ and $^{146}Nd/^{144}Nd = 0.7219$, respectively. The reported $^{87}Sr/^{86}Sr$ and $^{143}Nd/^{144}Nd$ ratios were adjusted to the NBS SRM 987 standard $^{87}Sr/^{86}Sr = 0.71025$ and the Shin Etsu JNdi-1 standard $^{143}Nd/^{144}Nd = 0.512115$.

4. Results

To determine the crystallization ages of the mafic rocks, one sample of each rock type was chosen for zircon U-Pb dating (supporting information Table S1). Major and trace element data for 65 rock samples obtained by this study and the literature data of the volcanic rocks from lower and upper parts of early Permian, and two samples from two different mafic dikes are listed in supporting information Table S3. Table 1 sets out

Table 1
Essential Diagnostic Geochemical Characteristics of Three Types Mafic Rocks

Diagnostic features	Calc-alkaline basalts (lower group of early Permian)	Shoshonitic basalts (upper group of early Permian)	Mafic dikes (intruded into early Permian strata)
Age (Ma)	~280 Ma	~272 Ma	~240 Ma
K_2O (wt %)	0.1–2.4	2.0–7.0	0.5–0.6
K_2O/Na_2O	0.01–0.8	0.5–2.1	0.08–0.11
Sr (ppm)	142–708	191–2,330	473–476
Ba (ppm)	14–600	891–2,701	71.5–91.7
La (ppm)	5.5–38.3	24.1–43.1	5.9–7.7
La/Yb	2.2–11.8	14.4–20.5	2.3–4.0
$\varepsilon_{Nd}(t)$	+1.9 to +7.4	+0.2 to +0.8	+3.5 to +3.9
Zircon $\varepsilon_{Hf}(t)$	+9.7 to +14.7	+2.8 to +4.9	+9.5 to +13.4
Mantle sources	Metasomatized asthenospheric mantle	Enriched lithospheric mantle	Depleted asthenospheric mantle
Geodynamic processes	Oceanic slab break-off	Subducted Tarim continental crust	Lithosphere thinning

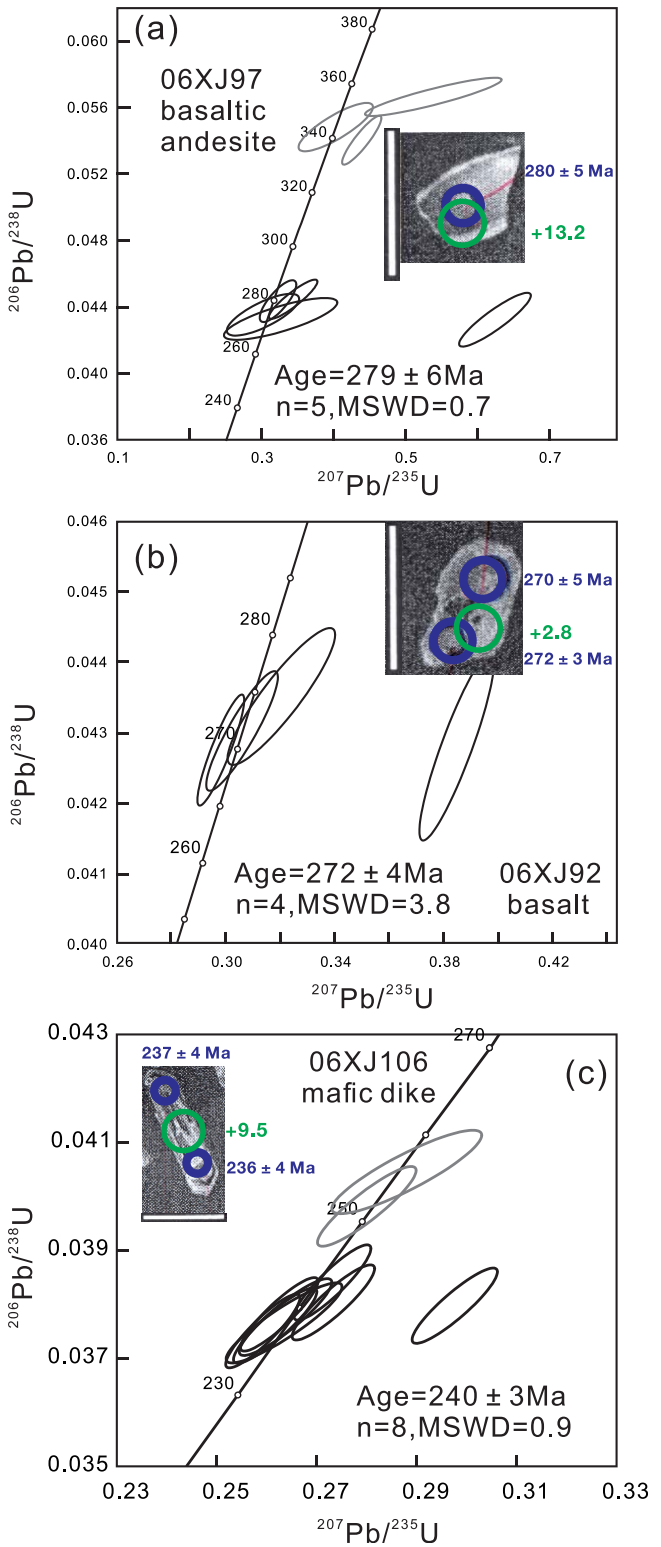

Figure 3. LA-ICP-MS zircon U-Pb Concordia diagrams with representative zircon CL images. The blue and green circles denote the analytical spots of U-Pb dating Lu-Hf isotopes ($\varepsilon_{Hf}(t)$), respectively. The scale bar in all CL image is 100 μm in length. The data sources are from supporting information Table S1.

the essential diagnostic geochemical features of the three types rocks. The sample locations and their stratigraphic positions are shown in Figure 1.

4.1. Zircon U-Pb Geochronology and Hf Isotopes

Five zircon analyses from basaltic andesite sample 06XJ97, from the lower part of the early Permian succession, and four from basalt 06XJ92, from the upper part of the succession, gave weighted mean $^{206}Pb/^{238}U$ ages of 279 ± 6 Ma (2σ) and 272 ± 4 Ma (2σ), respectively (Figures 3a and 3b). Five other analyses from sample 06XJ97 yielded $^{206}Pb/^{238}U$ ages of 1,839–340 Ma, which are interpreted as the ages of xenocrystic zircons entrained from country rocks.

Zircon grains from a mafic dike (06XJ106) are generally 50–100 μm in size and euhedral with concentric oscillatory zones, consistent with a magmatic origin. They have moderate Th and U contents ranging from 141 to 651 and 254 to 1,073 ppm, with consistent Th/U ratios (0.40–1.09). Eight analyses yield a weighted mean $^{206}Pb/^{238}U$ age of 240 ± 3 Ma (Figure 3c). This result is interpreted as the best estimate for the age of mafic dike crystallization.

The zircons from the lower group of Permian volcanic rocks (06XJ97) and the Triassic basaltic dike (06XJ106) have strongly depleted Hf isotopic composition, with $\varepsilon_{Hf}(t)$ values ranging from +9.8 to +14.7, and from +9.5 to +13.4, respectively. The from the upper lower group of Permian volcanic rocks (06XJ92) have distinct lower $\varepsilon_{Hf}(t)$ values of +2.8 to +4.9 (supporting information Table S2).

Mafic rocks may contain very few or no magmatic zircons but many xenocrystic grains. For the Awulale Permian mafic volcanic rocks, the xenocrystic zircons were likely derived from the Tianshan basement or Palaeozoic (Silurian-Carboniferous) magmatic rocks based on the age range from sample06XJ97 (supporting information Table S1). At the same time, the early Permian zircons from mafic volcanic rocks may be derived from coeval (~272 Ma) diorite and granodiorite porphyries that intruded into the early Permian volcanic-sedimentary formations (Tang et al., 2017b). However, the early Permian zircons that crystallized from the Awulale mafic volcanic rocks have an irregular or angular shape, and are weakly zoned with an otherwise homogeneous texture, similar to many zircons from mafic rocks (Corfu et al., 2003). Furthermore, the $\varepsilon_{Hf}(t)$ values of the early Permian zircons from the lower and upper groups of Awulale mafic volcanic rocks are distinctly higher and lower than those from the granodiorite porphyries (+5.4 to +11.2) (Tang et al., 2017b). This indicates to us that the early Permian zircons represent the age of crystallization of the mafic volcanic rocks, rather material incorporated from the granodiorite porphyries. The zircons from the mafic dike are elongated, showing oscillatory zonation, and have depleted Hf isotope composition ($\varepsilon_{Hf}(t)$ = +9.5 − +13.4), indicating that these zircons are magmatic and date the time of dike emplacement.

In summary, zircon U-Pb age results indicate that the analyzed Permian magmatic rocks were all emplaced over a short interval (~280 to 270 Ma), whereas the mafic dike formed during the Triassic (~240 Ma).

4.2. Whole-Rock Major and Trace Elements Geochemistry

The lower group of early Permian samples is mainly classified as basalt, trachybasalt, basaltic andesite, and basaltic trachyandesite on the total alkali-silica diagram (Le Maitre, 2002) (Figure 4a). On the K_2O versus SiO_2 diagram (Peccerillo & Taylor, 1976) (Figure 4b), the samples mainly

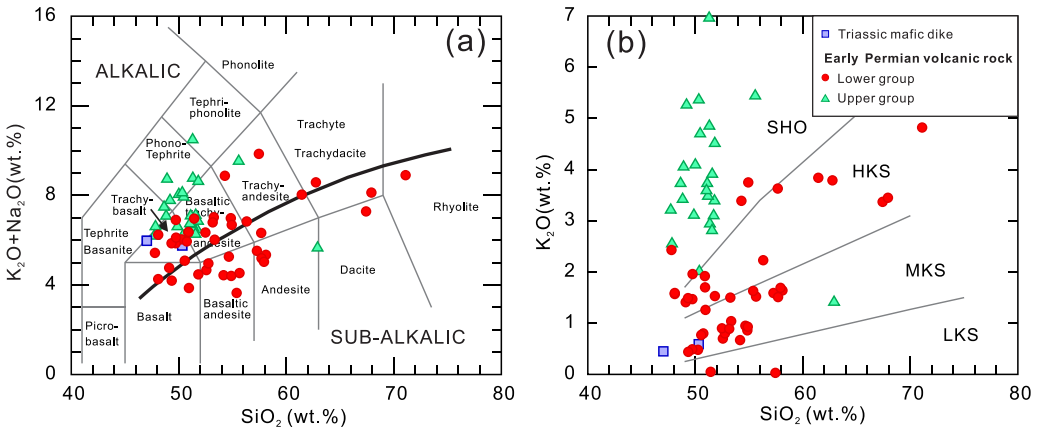

Figure 4. (a) Total alkalis versus SiO_2 diagram (Le Maitre, 2002), the dashed line separating alkaline series from subalkaline series is from Irvine and Baragar (1971). (b) K_2O versus SiO_2 diagram Peccerillo and Taylor (1976), LKS, MKS, HKS, and SHO are low-K tholeiite series, medium-K calc-alkaline series, high-K calc-alkaline series, and shoshonitic series, respectively. The data sources are from supporting information Table S3.

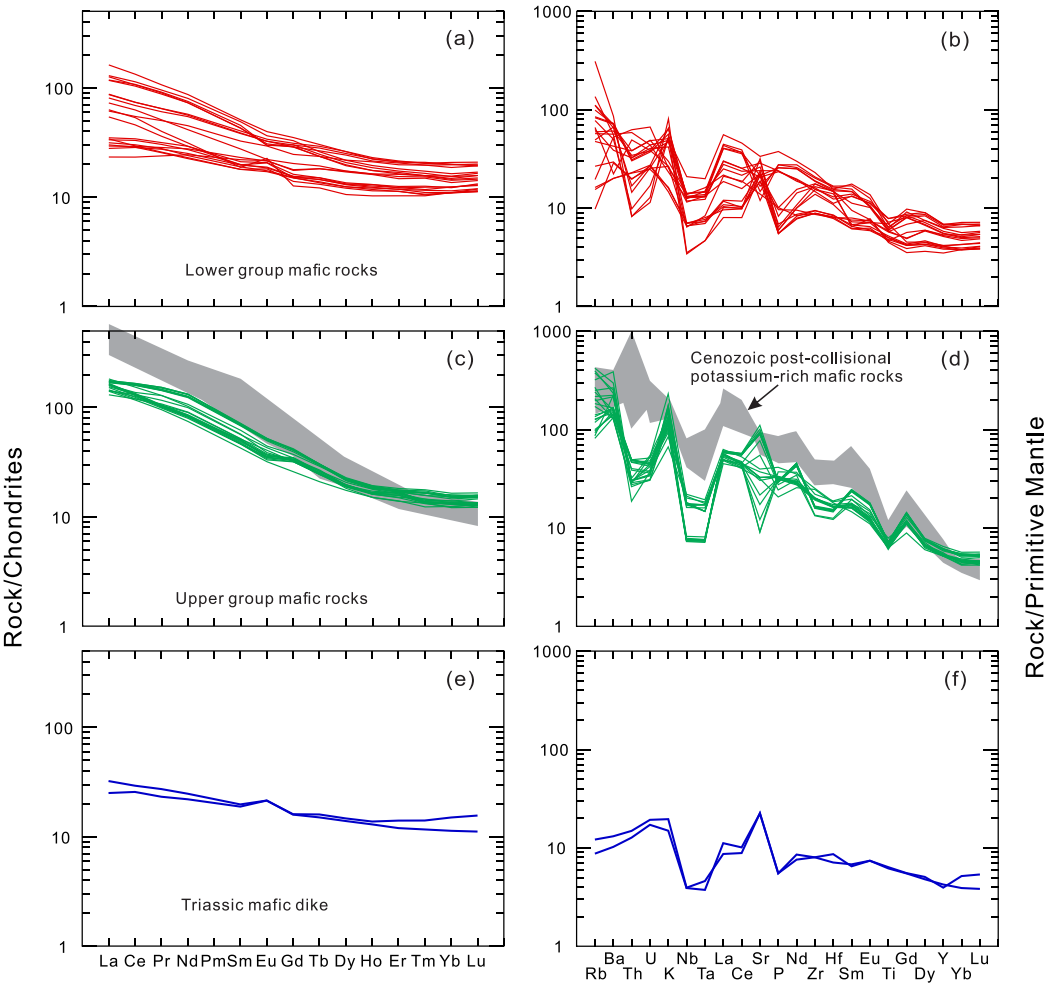

Figure 5. Chondrite-normalized rare earth element patterns and primitive mantle-normalized multielement diagram for the early Permian-Triassic magmatic rocks of the Awulale Mountains. Chondrite and primitive mantle normalizing values are from Sun and McDonough (1989). Cenozoic postcollisional potassium-rich mafic rocks (Guo et al., 2014) are shown for comparision. The data sources are same as Figure 4.

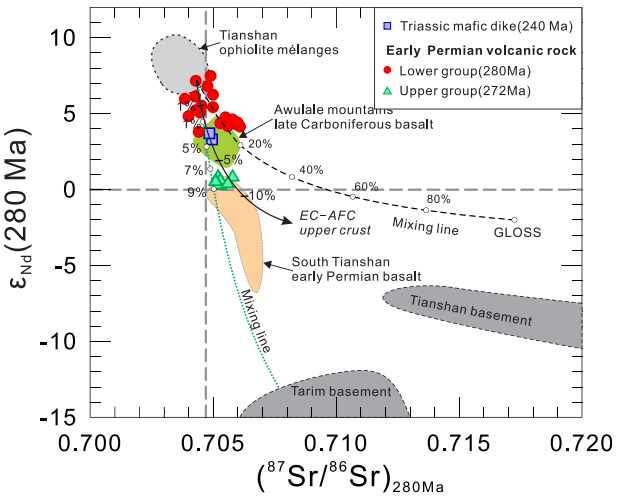

Figure 6. $(^{87}Sr/^{86}Sr)_i$ versus $\varepsilon_{Nd}(t)$ diagram showing two-component mixing and EC-AFC calculations. The Sr-Nd isotope data of Tianshan ophiolites (Xu et al., 2006); late Carboniferous basalts from the Awulale Mountains (Li et al., 2015; Tang et al., 2014; Yan et al., 2015) and South Tianshan early Permian basalts (Huang et al., 2015; Liu et al., 2014) are shown for comparision. Tarim Archean and Neoproterozoic basement are from Cao et al. (2011). Tianshan Neoproterozoic basement are from Chen et al. (1999). Data for global subducting sediment (GLOSS) are from Plank and Langmuir (1988). The modeling parameters are listed in supporting information Table S3. Small circles on the curves indicate the percentage of assimilated contaminant. The other data sources and symbols are same as Figure 4.

plot along a calc-alkaline differentiation trend with medium- to high-K characteristics. In contrast, the upper group of early Permian volcanic rocks consists mainly of trachybasalt, basaltic trachyandesite, and phonotephrite, and all mafic samples are shoshonitic.

The basaltic rocks from the lower group rocks have rare earth element (REE) patterns with slight enrichment of the light REE (LREE) and relatively little variation in the heavy REE (HREE) (La/Yb = 2.2–11.8) (Figure 5a). They have moderately negative to slightly positive Eu anomalies (Eu/Eu* ($2*Eu_N/(Sm + Gd)_N$) = 0.6–1.1). In contrast to the lower group, the upper group basaltic rocks are characterized by strong LREE enrichment and steep REE patterns (La/Yb = 14.4–20.5), with negligible Eu anomalies (Eu/Eu* = 0.86–0.98) (Figure 5c). Both groups of basaltic rocks are enriched in large-ion lithophile elements (LILE: Rb, Ba, Th, U, K), but are depleted in Nb, Ta, P, and Ti relative to neighboring REE (Figure 5). In general, the upper group rocks have higher incompatible element concentrations than the lower group. In detail, the upper group basaltic rocks have higher Nb/Ta ratios (17.4–21.6) and Zr/Hf ratios (42.4–49.6) than those of the lower group basaltic rocks (Nb/Ta = 12.8–18.4; Zr/Hf = 36.2–43.6). Both groups of volcanic rocks show distinct negative Nb-Ta anomalies in their mantle-normalized patterns, with Nb/La ratios ranging from 0.32 to 0.75 for lower group and from 0.13 to 0.43 for upper group basaltic rocks (supporting information Table S3).

The Triassic mafic dikes are characterized by low SiO_2 (47.0–50.3 wt %) and K_2O contents (0.45–0.59 wt %) that plot in the medium-K calc-alkaline field (Figure 4b). They have low La/Yb ratios from 2.3 to 3.9, slight enrichment of the LREE and less variation of the HREE. In general, the trace elements patterns of the Triassic mafic dikes parallel those of the Permian lower group basaltic rocks (Figure 5).

4.3. Nd-Sr Isotopic Compositions

The two groups of Permian volcanic rocks have distinctly different $\varepsilon_{Nd}(t)$ values of +1.9 to +7.4 and +0.2 to +0.8 for the low and upper group rocks, respectively (Figure 6). The lower group basaltic rocks have a wide range of initial $^{87}Sr/^{86}Sr$ values (0.7039–0.7068), whereas the upper group samples tend to be more radiogenic and with a smaller range of initial $^{87}Sr/^{86}Sr$ values (0.7052–0.7062) (Figure 6). Triassic basaltic dikes have initial $^{87}Sr/^{86}Sr$ and $\varepsilon_{Nd}(t)$ ranging from 0.7048 to 0.7049 and +3.5 to +3.9, respectively, similar to the early Permian lower group basaltic rocks (Figure 6).

5. Discussion

5.1. Petrogenesis of the Early Permian Lower Group Calc-Alkaline Rocks

5.1.1. Crustal Contamination

The occurrence of Paleoproterozoic zircons in the calc-alkaline, lower Permian group rocks indicates that their parental magmas were subject to crustal contamination (supporting information Table S1). To further assess the role of crustal assimilation in these rocks, we used the energy-constrained assimilation and fractional crystallization (EC-AFC) model of Spera and Bohrson (2001), applied to $(^{87}Sr/^{86}Sr)_i$ versus $\varepsilon_{Nd}(t)$ (Figure 6). Supporting information Table S4 shows the thermal and geochemical input parameters employed. The physical characteristics of the magma body-country rock system are those suggested by Bohrson and Spera (2001) for standard upper crust. The Sr-Nd elemental and isotopic compositions of crustal contaminant are inferred based on the Neoproterozoic gneissic granite from the central part of Tianshan, considered to be a good proxy for the local upper crust (Chen et al., 1999; Hu et al., 2010). The output from EC-AFC simulation provides model curves to fit the correlation trends between $(^{87}Sr/^{86}Sr)_i$ and $\varepsilon_{Nd}(t)$ (Figure 6), although $\varepsilon_{Nd}(t)$ values are scattered, presumably reflecting variations in the composition of country rock and/or the least differentiated basalts. Our modeling indicates that small amounts of crustal contamination (<5%) could produce the Sr-Nd isotope variation for most of the lower group samples.

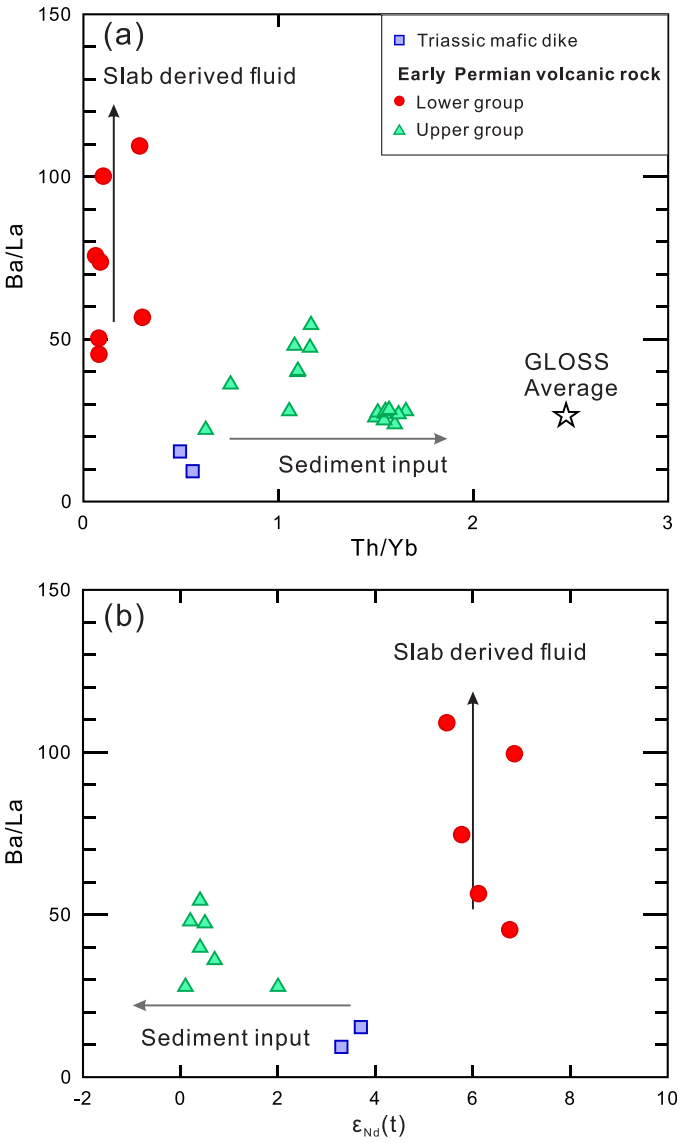

Figure 7. (a) Ba/La versus Th/Yb and (b) Ba/La versus $\varepsilon_{Nd}(t)$ plots. GLOSS average are from Plank and Langmuir (1998). The data sources and symbols are same as Figure 4.

To minimize the effects of AFC processes, only those samples with primary mantle values, including depleted Nd-Sr isotope compositions ($(^{87}Sr/^{86}Sr)_i < 0.705$, $\varepsilon_{Nd}(t) > +5.5$) and high MgO contents (>6.6 wt %), are considered in discussion of the mantle source.

5.1.2. Mantle Source and Subduction Components

The most distinctive geochemical feature of the lower group basaltic rocks is the LILE enrichment and the presence of strongly negative Nb and Ta anomalies in primitive mantle (PM)-normalized trace element patterns (Figure 5), suggesting slab-derived enrichments in their source. Thus, the primary magma of the lower group basaltic rocks are interpreted as the product of partial melting of metasomatized subcontinental lithospheric mantle (SCLM) or derived from a depleted mantle wedge enriched by previous Paleozoic subduction-related components, including fluids dehydrated from subducted oceanic slab or subducted sediments (Hawkesworth et al., 1993, 1997; Tatsumi et al., 1986). All of the lower group basaltic rocks have much higher Ba/La than global subducting sediment (GLOSS) with low Th/Yb (Figure 7a), indicating significantly more influence from fluids (Woodhead et al., 2011) rather than bulk sediment or a partial melt of subducted sediment (Hawkesworth et al., 1997). Furthermore, on a Ba/La versus $\varepsilon_{Nd}(t)$ diagram (Figure 7b), lower group basaltic rocks fall in the high $\varepsilon_{Nd}(t)$ and Ba/La field, which is also consistent with moderate fluid-induced enrichment rather than sediment input. The Nd-Sr isotope compositions of the parental magmas of the lower Permian rocks are remarkably different from the late Carboniferous basaltic rocks in the Awulale Mountains (Figure 6). For example, they have distinctly higher $\varepsilon_{Nd}(t)$ values than that of late Carboniferous basalt from the same region, close to the Tianshan ophiolites (Figure 6). Thus, the geochemical and isotopic evidence suggests that the lower group of early Permian rocks were derived from an asthenospheric mantle that had been metasomatized by fluids derived from previous subducted oceanic slab, which is common for calc-alkaline rocks (Harangi et al., 2007).

5.2. Petrogenesis of the Early Permian Upper Group K-Rich Rock

The upper group samples all have relatively high $(^{87}Sr/^{86}Sr)_i$ and low $\varepsilon_{Nd}(t)$, which differs from typical late Carboniferous basalts from the Awulale Mountains (Figure 6). Crustal contamination is considered unlikely to have occurred in these samples as it fails to explain the limited range of values and the absence of older inherited zircon. Crustal contamination can also be excluded owing to the lack of coupled variations between Sr and Nd isotope ratios and major elements, such as MgO and SiO_2 versus $^{87}Sr/^{86}Sr$ and $\varepsilon_{Nd}(t)$ (supporting information Table S3).

The enriched Nd-Sr isotope compositions, together with the strong enrichment in incompatible elements, of the upper group basaltic rocks are typical features of shoshonitic rocks (Figures 5 and 6). Most studies ascribe mantle-derived shoshonitic magmas to derivation via low-degree partial melting of SCLM enriched by subduction-related fluid and/or melts (Foley, 1992; Hawkesworth & Vollmer, 1979; Kirchenbaur et al., 2012; Turner et al., 1996; Wyman & Kerrich, 1993; Yang et al., 2007). The upper group basaltic rocks have low Ba/La and high Th/Yb ratios (Figure 7), indicating significant input of subducted sediment. However, the mixing modeling line for this simple model trends away from the data array (Figure 6). If more depleted Sr isotope compositions are selected for the lithospheric mantle to achieve the observed Sr-Nd isotope trends, then assimilation of more than 40% of GLOSS is required. Such a high percentage of sediments cannot be reconciled with the basaltic composition of the upper group rocks. Therefore, oceanic sediment input is even less likely as a suitable source for the enrichment mantle sources for the upper group rocks than for the lower group rocks.

The upper group basaltic rocks are comparable with the Cenozoic postcollisional potassium-rich mafic magmatism in the Tibetan plateau that have been interpreted to represent derivation from enriched lithospheric mantle metasomatized by subducted Indian continental crust (e.g., Ding et al., 2003; Guo et al., 2013; Mahéo et al., 2002; Zhao et al., 2009) (Figure 5). In addition, the trace element characteristics, such as Sm/Nd (0.19) and Th/U (3.67), which are similar to typical upper continental crustal values (Sm/Nd = 0.17, Th/U = 3.89; Rudnick & Gao, 2003), indicate that upper continental-derived materials were involved in the mantle sources for the upper group basaltic rocks. As discussed above, crustal contamination could not govern the geochemical characteristics of the upper group sample set. Thus, we propose that they originated from enriched Tianshan SCLM sources metasomatized by subduction of the continent crust.

The final collision between the Tarim Craton and the Yili-Central Tianshan along the southern margin of to the CAOB occurred at the end of the late Carboniferous. This collision is indicated geochemically by an abrupt change from depleted mantle-type to enriched continental-type zircon Hf isotope compositions for Yili-Central Tianshan arc granitoids at ~300 Ma (Tang et al., 2017a). Furthermore, seismic reflection data across the region has been interpreted to indicate the presence of Tarim continental crust extending beneath the Tianshan Orogen to distances of 50–100 km (Makarov et al., 2010). It seems likely that the Tarim continental crust was underthrust beneath the Yili-Central Tianshan during early Permian, which significantly altered the chemical composition of any preexisting relatively depleted mantle lithosphere.

In the $(^{87}Sr/^{86}Sr)_i$ versus $\varepsilon_{Nd}(t)$ plot (Figure 6), the Awulale upper group rocks, coupled with the South Tianshan early Permian basalts, point to the involvement of ancient continental crust material, which we identify as Tarim basement characterized by very enriched Sr-Nd isotopic compositions (Cao et al., 2011). Binary mixing, between end-members of Tarim basement and a depleted mantle source represented by the Tianshan ophiolites, shows that assimilation of ~8% Tarim basement can generate the isotopic array of the Awulale upper group rocks (Figure 6). Thus, the lithospheric mantle sources for the upper group rocks were metasomatized by the Tarim continental crustal component. This hypothesis of mantle metasomatism through subduction of Tarim continental margin lithosphere is also supported by the transition from subalkaline to alkaline and shoshonitic volcanism in the Awulale Mountains, and the trend toward more enriched Nd isotope compositions during early Permian (Figure 6).

5.3. Petrogenesis of the Middle Triassic Mafic Dike

The Triassic mafic dikes have similar REE and other trace elements patterns, as well as Sr-Nd isotope compositions, compared to the lower group samples (Figures 4–6). We are cautious about drawing too many conclusions based on two samples, but we consider their petrogenesis likely involved melting of asthenosphere mantle sources similar to the lower group basaltic rocks.

5.4. Transition in Mantle Sources in a Postcollisional Tectonic Setting

The lower group volcanic rocks from the Awulale Mountains are characterized by low La/Yb ratios and depleted Sr-Nd isotope compositions (Figures 5 and 6), indicating they originated from a asthenospheric mantle source at a shallow level. Thus, their genesis reflects upwelling asthenosphere in an extensional geodynamic setting. At the same time, significant uplift occurred in the Tianshan Orogen as indicated by accumulation of the lower Permian red molasse, interpreted to reflect an extensional setting during this time (Han et al., 2011). The lower group volcanic rocks are coeval with the early Permian (~290 to 280 Ma) A-type granites from the Tianshan Orogen (e.g., Konopelko et al., 2007; Seltmann et al., 2011; Tang et al., 2010; Yuan et al., 2010). Thus, the early Permian lower group basalts from the Awulale Mountains, coupled with coeval A-type granites, are attributed to oceanic slab break-off following closure of the Paleo-Asian ocean at about 300 Ma (Han et al., 2011; Tang et al., 2010; Yuan et al., 2010). Oceanic slab break-off generally occurs in the early stages of continental collision (von Blanckenburg & Davies, 1995). In the slab break-off model, hot asthenospheric mantle rises generating a transitory thermal anomaly in the mantle wedge. Partial melting of the upwelling depleted asthenospheric mantle at a shallow level would produce the lower group volcanic rocks. In addition, the thermal anomaly could trigger partial melting of the lower crust, leading to generation of the coeval A-type granites.

A possible model would involve a initial collision and attemoted subduction of Tarim continental crust with the Tianshan arc in which a depleted asthenospheric source evolves to an enriched lithospheric mantle source. Melting of the enriched lithosphere produces the upper group K-rich magma in the Awulale

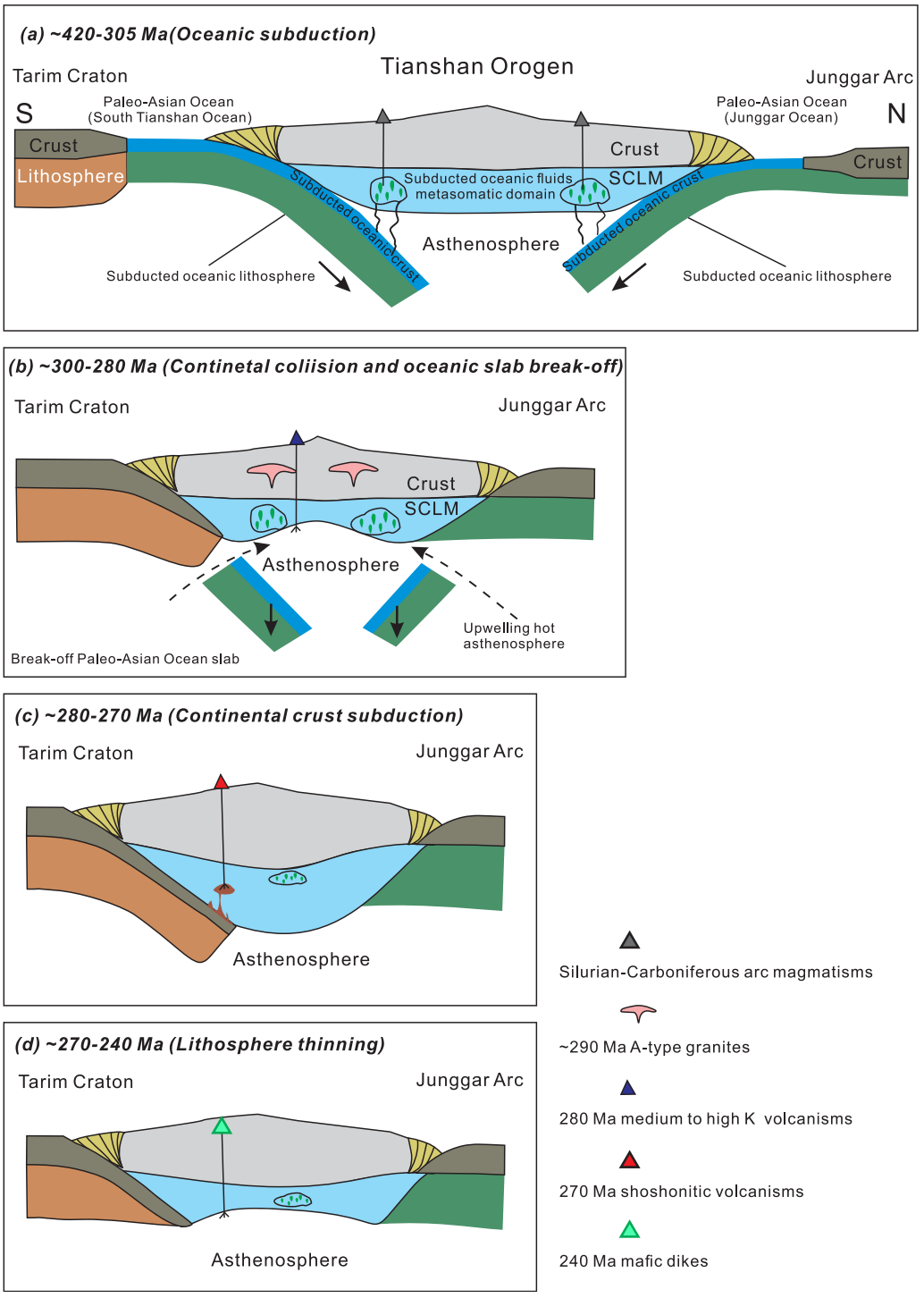

Figure 8. Schematic illustration of the tectonic evolution of the Chinese western Tianshan Orogen and proposed model for the origin of the various early Permian and Triassic (290–240 Ma) mantle and crustal-derived magmatic suites in the Awulale Mountains.

Mountains (Figure 8). Subduction of the Tarim continental crust during collision would also lead to thickening of the lithospheric mantle and crust in the overriding Yili-Central Tianshan arc of the Tianshan Orogen. In the second stage, during the middle Triassic, which is after the termination of collision between the Tarim Craton and Yili-Central Tianshan arc, the enriched lithospheric source is replaced by depleted

asthenospheric mantle through convective thinning or delamination (Bird, 1979; Houseman et al., 1981) (Figure 8). In addition to the Triassic mafic dikes in the Awulale Mountains, Triassic mafic rocks are occur sporadically in the east and southwest Tiansan regions (e.g., Wu et al., 2010), which is consistent with lithosphere thinning in a postcollisional setting.

Transition in mantle sources as proposed for the Palaeozoic history of Awulale Muntains is a common feature during the tectonic evlotion of orogenic belts such as the Andes (e.g., Kay et al., 1994), western North America (e.g., Manthei et al., 2010), and the Tibetan plateau (e.g., Chung et al., 2005). The tranistion in mantle sources from enriched to depleted is inferred to be induced by oceanic subduction (Collins et al., 2011), slab-rollback (Best et al., 2016), or lithospheric delamination (DeCelles et al., 2009; Lee & Anderson, 2015). The subsequent reversion from depleted to enriched mantle sources probably reflects subduction erosion (von Huene & Scholl, 1991) or the continental subduction (Chu et al., 2011). Thus, our study of the geochemical and isotopic characteristics of the mafic rocks of the Tainshan Orogen further documents the evolution of mantle sources in a postcollisional orogenic setting.

6. Conclusions

1. Postcollisional magmatic activity in the Awulale Mountains, Tianshan Orogen, yields early Permian and Triassic ages with the former divisable into lower and upper successions.
2. The lower group of early Permian magmas is calc-alkaline basalts derived from melting of a depleted asthenospheric mantle metasomatized by fluids from the previous subducted oceanic slab followed by upper crustal contamination.
3. The early Permian upper group is shonshonitic rocks generated by melting of enriched lithospheric mantle.
4. Middle Triassic mafic dikes are interpreted as the product of partial melting of a depleted asthenospheric mantle source similar to the early Permian lower group basaltic rocks.
5. The early Permian transition in mantle chemistry from depleted asthenospheric mantle sources to enriched lithospheric mantle corresponds with closure of the Paleo-Asian ocean and partial subduction of the Tarim continental crust beneath the Yili-Central Tianshan arc, resulting in thickening of the upper plate lithosphric mantle. Subsequent derivation of Traissic basalts from asthenospheric mantle source is interpreted to reflect late-stage postcollisional thinning of the lithospheric mantle beneath the Tianshan Orogen.

Acknowledgments
We are grateful to Chris Hawkesworth for thoughtful and constructive comments on an early version of the manuscript. We also thank journal Editor Cin-Ty Lee and two anonymous reviewers for comments that helped clarify our ideas and their significance. We thank Yongshen Liu, Ying Liu, and Xirong Liang for their assistance with laboratory work. This work was supported by funding from the Strategic Priority Research Program (B) of the Chinese Academy of Sciences (grant XDB18020204 and XDB03010600), the National Natural Science Foundation of China (grant 41673033, 41630208, and 41202041), the Key Program of the Chinese Academy of Sciences (QYZDJ-SSW-DQC026), and GIGCAS 135 project 135TP201601. Peter Cawood acknowledges support from the Natural Environment Research Council (grant NE/J021822/1) and from the Australian Research Council (grant FL160100168). The senior author thanks the NSC, Taiwan, for a grant which supported his 1 year academic visit at the NTU. This is contribution no. IS-2466 from GIG–CAS. All data are available in the supporting information.

References

Allen, M. B., Kheirkhah, M., Neill, I., Emami, M. H., & Mcleod, C. L. (2013). Generation of Arc and within-plate chemical signatures in collision zone magmatism: Quaternary lavas from Kurdistan Province, Iran. *Journal of Petrology*, *54*(5), 887–911.

Best, M. G., Christiansen, E. H., de Silva, S., & Lipman, P. W. (2016). Slab-rollback ignimbrite flareups in the southern Great Basin and other Cenozoic American arcs: A distinct style of arc volcanism. *Geosphere*, *12*(4), 1097–1135.

Bird, P. (1979). Continental delamination and the Colorado Plateau. *Journal of Geophysical Research*, *84*(B13), 7561–7571.

Bohrson, W. A., & Spera, F. J. (2001). Energy-constrained open-system magmatic processes II: Application of Energy-Constrained Assimilation–Fractional Crystallization (EC-AFC) model to magmatic systems. *Journal of Petrology*, *42*(5), 1019–1041.

Cao, X., Lü, X., Liu, S., Zhang, P., Gao, X., Chen, C., & Mo, Y. (2011). LA-ICP-MS zircon dating, geochemistry, petrogenesis and tectonic implications of the Dapingliang Neoproterozoic granites at Kuluketage block, NW China. *Precambrian Research*, *186*(1–4), 205–219.

Carlson, R. W., Pearson, D. G., & James, D. E. (2005). Physical, chemical, and chronological characteristics of continental mantle. *Reviews of Geophysics*, *43*, RG1001. https://doi.org/10.1029/2004RG000156

Chen, G. W., Deng, T., Liu, R., Xia, H., & Liu, Q. (2015). Geochemistry of bimodal vocanic rocks in Permian Taerdetao Formation in Awulale area of western Tiashan, Xinjiang. *Acta Petrologica Sinica*, *31*(1), 105–118.

Chen, Y. B., Hu, A., Zhang, G. X., & Zhang, Q. F. (1999). Precambrian basement age and characteristics of Southwestern Tianshan: Zircon U-Pb geochronology and Nd-Sr isotopic compositions. *Acta Petrologica Sinica*, *16*(1), 91–98.

Chu, M.-F., Chung, S.-L., O'reilly, S. Y., Pearson, N. J., Wu, F.-Y., Li, X.-H., . . . Lee, H.-Y. (2011). India's hidden inputs to Tibetan orogeny revealed by Hf isotopes of Transhimalayan zircons and host rocks. *Earth and Planetary Science Letters*, *307*(3–4), 479–486.

Chung, S. L., Chu, M. F., Zhang, Y. Q., Xie, Y. W., Lo, C. H., Lee, T. Y., . . . Wang, Y. Z. (2005). Tibetan tectonic evolution inferred from spatial and temporal variations in post-collisional magmatism. *Earth-Science Reviews*, *68*(3–4), 173–196.

Collins, W. J., Belousova, E. A., Kemp, A. I. S., & Murphy, J. B. (2011). Two contrasting Phanerozoic orogenic systems revealed by hafnium isotope data. *Nature Geoscience*, *4*(5), 333–337.

Corfu, F., Hanchar, J. M., Hoskin, P. W. O., & Kinny, P. (2003). Atlas of zircon textures. *Reviews in Mineralogy and Geochemistry*, *53*(1), 469–500.

DeCelles, P. G., Ducea, M. N., Kapp, P., & Zandt, G. (2009). Cyclicity in Cordilleran orogenic systems. *Nature Geoscience*, *2*(4), 251–257.

Ding, L., Kapp, P., Zhong, D., & Deng, W. (2003). Cenozoic volcanism in Tibet: Evidence for a transition from oceanic to continental subduction. *Journal of Petrology*, *44*(10), 1833–1865.

Foley, S. (1992). Vein-plus-wall-rock melting mechanisms in the lithosphere and the origin of potassic alkaline magmas. *Lithos*, *28*(3–6), 435–453.

Gao, J., Klemd, R., Qian, Q., Zhang, X., Li, J., Jiang, T., & Yang, Y. (2011). The collision between the Yili and Tarim blocks of the Southwestern Altaids: Geochemical and age constraints of a leucogranite dike crosscutting the HP–LT metamorphic belt in the Chinese Tianshan Orogen. *Tectonophysics*, *499*(1–4), 118–131.

Guo, Z., Cheng, Z., Zhang, M., Zhang, L., Li, X., & Liu, J. (2015a). Post-collisional high-K calc-alkaline volcanism in Tengchong volcanic field, SE Tibet: Constraints on Indian eastward subduction and slab detachment. *Journal of the Geological Society*, *172*(5), 624–640.

Guo, Z., Wilson, M., Zhang, M., Cheng, Z., & Zhang, L. (2013). Post-collisional, K-rich mafic magmatism in south Tibet: Constraints on Indian slab-to-wedge transport processes and plateau uplift. *Contributions to Mineralogy and Petrology*, *165*(6), 1311–1340.

Guo, Z., Wilson, M., Zhang, M., Cheng, Z., & Zhang, L. (2015b). Post-collisional Ultrapotassic Mafic Magmatism in South Tibet: Products of partial melting of pyroxenite in the mantle wedge induced by roll-back and delamination of the subducted Indian continental lithosphere slab. *Journal of Petrology*, *56*(7), 1365–1406.

Guo, Z., Wilson, M., Zhang, L., Zhang, M., Cheng, Z., & Liu, J. (2014). The role of subduction channel mélanges and convergent subduction systems in the petrogenesis of post-collisional K-rich mafic magmatism in NW Tibet. *Lithos*, *198–199*, 184–201.

Guo, Z. F., Wilson, M., Liu, J. Q., & Mao, Q. (2006). Post-collisional, potassic and ultrapotassic magmatism of the northern Tibetan Plateau: Constraints on characteristics of the mantle source, geodynamic setting and uplift mechanisms. *Journal of Petrology*, *47*(6), 1177–1220.

Han, B.-F., He, G.-Q., Wang, X.-C., & Guo, Z.-J. (2011). Late carboniferous collision between the Tarim and Kazakhstan–Yili terranes in the western segment of the South Tian Shan Orogen, Central Asia, and implications for the Northern Xinjiang, western China. *Earth-Science Reviews*, *109*(3–4), 74–93.

Harangi, S., Downes, H., Thirlwall, M., & Gméling, K. (2007). Geochemistry, petrogenesis and geodynamic relationships of miocene calc-alkaline volcanic rocks in the western Carpathian Arc, eastern central Europe. *Journal of Petrology*, *48*(12), 2261–2287.

Hawkesworth, C. J., Gallagher, K., Hergt, J. M., & McDermott, F. (1993). Mantle and slab contributions in arc magmas. *Annual Review of Earth and Planetary Sciences*, *21*(1), 175–204.

Hawkesworth, C. J., Turner, S. P., McDermott, F., Peate, D. W., & van Calsteren, P. (1997). U-Th isotopes in arc magmas: Implications for element transfer from the subducted crust. *Science*, *276*(5312), 551–555.

Hawkesworth, C. J., & Vollmer, R. (1979). Crustal contamination versus enriched mantle: 143Nd/144Nd and 87Sr/86Sr evidence from the Italian volcanics. *Contributions to Mineralogy and Petrology*, *69*(2), 151–165.

Houseman, G. A., McKenzie, D. P., & Molnar, P. (1981). Convective instability of a thickened boundary layer and its relevance for the thermal evolution of continental convergent belts. *Journal of Geophysical Research*, *86*(B7), 6115–6132.

Hu, A. Q., Wei, G. J., Jahn, B. M., Zhang, J. B., Deng, W. F., & Chen, L. L. (2010). Formation of the 0.9Ga Neoproterozoic granitoids in the Tianshan Orogen, NW China: Constraints from the SHRIMP zircon age determination and its tectonic significance. *Geochimica*, *39*(3), 197–212.

Huang, H., Zhang, Z., Santosh, M., Zhang, D., & Wang, T. (2015). Petrogenesis of the early Permian volcanic rocks in the Chinese South Tianshan: Implications for crustal growth in the Central Asian Orogenic Belt. *Lithos*, *228–229*, 23–42.

Irvine, T. N., & Baragar, W. R. A. (1971). A guide to the chemical classification of the common volcanic rocks. *Canadian Journal of Earth Sciences*, *8*(5), 523–548.

Kay, S. M., Coira, B., & Viramonte, J. (1994). Young mafic back arc volcanic rocks as indicators of continental lithospheric delamination beneath the Argentine Puna Plateau, central Andes. *Journal of Geophysical Research*, *99*(B12), 24323–24339.

Kirchenbaur, M., Münker, C., Schuth, S., Garbe-Schönberg, D., & Marchev, P. (2012). Tectonomagmatic constraints on the sources of eastern Mediterranean K-rich lavas. *Journal of Petrology*, *53*(1), 27–65.

Konopelko, D., Biske, G., Seltmann, R., Eklund, O., & Belyatsky, B. (2007). Hercynian post-collisional A-type granites of the Kokshaal Range, Southern Tien Shan, Kyrgyzstan. *Lithos*, *97*(1–2), 140–160.

Lee, C.-T. A., & Anderson, D. L. (2015). Continental crust formation at arcs, the arclogite "delamination" cycle, and one origin for fertile melting anomalies in the mantle. *Science Bulletin*, *60*(13), 1141–1156.

Le Maitre, R. W (2002). *Igneous rocks: A classification and glossary of terms* (236 pp.). Cambridge, UK: Cambridge University Press.

Li, N.-B., Niu, H.-C., Zhang, X.-C., Zeng, Q.-S., Shan, Q., Li, C.-Y., . . .Yang, W.-B. (2015). Age, petrogenesis and tectonic significance of the ferrobasalts in the Chagangnuoer iron deposit, western Tianshan. *International Geology Review*, *57*(9–10), 1218–1238.

Li, X. H., Li, Z. X., Wingate, M. T. D., Chung, S. L., Liu, Y., Lin, G. C., & Li, W. X. (2006). Geochemistry of the 755Ma Mundine Well dyke swarm, northwestern Australia: Part of a Neoproterozoic mantle superplume beneath Rodinia? *Precambrian Research*, *146*(1–2), 1–15.

Lin, W., Chu, Y., Ji, W., Zhang, Z., Shi, Y., Wang, Z., . . . Wang, Q. (2013). Geochronological and geochemical constraints for a middle Paleozoic continental arc on the northern margin of the Tarim block: Implications for the Paleozoic tectonic evolution of the South Chinese Tianshan. *Lithosphere*, *5*(4), 355–381.

Liu, D., Guo, Z., Jolivet, M., Cheng, F., Song, Y., & Zhang, Z. (2014). Petrology and geochemistry of Early Permian volcanic rocks in South Tian Shan, NW China: Implications for the tectonic evolution and Phanerozoic continental growth. *International Journal of Earth Sciences*, *103*(3), 737–756.

Long, L., Gao, J., Klemd, R., Beier, C., Qian, Q., Zhang, X., . . . Jiang, T. (2011). Geochemical and geochronological studies of granitoid rocks from the Western Tianshan Orogen: Implications for continental growth in the southwestern Central Asian Orogenic Belt. *Lithos*, *126*(3–4), 321–340.

Ludwig, K. R. (2003). User's manual for Isoplot 3.00: A geochronological toolkit for Microsoft Excel, *Berkeley Geochronology Center Special Publication*, *4*, 1–70.

Luo, Y., Shan, Q., Zeng, Q. S., Li, N. B., Jiang, Y. H., & Zeng, L. J. (2013). Geochemistry of Permian potassic mafic volcanic rocks in western Awulale Mountains. *Geochimica*, *42*(6), 544–556.

Lustrino, M., Duggen, S., & Rosenberg, C. L. (2011). The Central-Western Mediterranean: Anomalous igneous activity in an anomalous collisional tectonic setting. *Earth-Science Reviews*, *104*(1–3), 1–40.

Mahéo, G., Guillot, S., Blichert-Toft, J., Rolland, Y., & Pêcher, A. (2002). A slab breakoff model for the Neogene thermal evolution of South Karakorum and South Tibet. *Earth and Planetary Science Letters*, *195*(1–2), 45–58.

Makarov, V. I., Alekseev, D. V., Batalev, V. Y., Bataleva, E. A., Belyaev, I. V., Bragin, V. D., . . . Shchelochkov, G. G. (2010). Underthrusting of Tarim beneath the Tien Shan and deep structure of their junction zone: Main results of seismic experiment along MANAS Profile Kashgar-Song-Köl. *Geotecton*, *44*(2), 102–126.

Manthei, C. D., Ducea, M. N., Girardi, J. D., Patchett, P. J., & Gehrels, G. E. (2010). Isotopic and geochemical evidence for a recent transition in mantle chemistry beneath the western Canadian Cordillera. *Journal of Geophysical Research*, *115*, B02204. https://doi.org/10.1029/2009JB006562

Martin, R. F., & Piwinskii, A. J. (1972). Magmatism and tectonic settings. *Journal of Geophysical Research*, *77*(26), 4966–4975.

Murphy, J. B., & Dostal, J. (2007). Continental mafic magmatism of different ages in the same terrane: Constraints on the evolution of an enriched mantle source. *Geology*, *35*(4), 335–338.
Neill, I., Meliksetian, K., Allen, M. B., Navasardyan, G., & Kuiper, K. (2015). Petrogenesis of mafic collision zone magmatism: The Armenian sector of the Turkish–Iranian Plateau. *Chemical Geology*, *403*, 24–41.
Peccerillo, A., & Taylor, S. R. (1976). Geochemistry of Eocene calc-alkaline volcanic rocks from the Kastamonu area, Northern Turkey. *Contributions to Mineralogy and Petrology*, *58*(1), 63–81.
Plank, T., & Langmuir, C. H. (1988). An evaluation of the global variations in the major element chemistry of arc basalts. *Earth and Planetary Science Letters*, *90*(4), 349–370.
Plank, T., & Langmuir, C. H. (1998). The chemical composition of subducting sediment and its consequences for the crust and mantle. *Chemical Geology*, *145*(3–4), 325–394.
Prelević, D., Stracke, A., Foley, S. F., Romer, R. L., & Conticelli, S. (2010). Hf isotope compositions of Mediterranean lamproites: Mixing of melts from asthenosphere and crustally contaminated mantle lithosphere. *Lithos*, *119*(3–4), 297–312.
Rudnick, R. L., & Gao, S. (2003). The composition of the continental crust. In R. L. Rudnick (Ed.), *The Crust* (pp. 1–64). Oxford, UK: Elsevier–Pergamon.
Seltmann, R., Konopelko, D., Biske, G., Divaev, F., & Sergeev, S. (2011). Hercynian post-collisional magmatism in the context of Paleozoic magmatic evolution of the Tien Shan orogenic belt. *Journal of Asian Earth Sciences*, *42*(5), 821–838.
Spera, F. J., & Bohrson, W. A. (2001). Energy-constrained open-system magmatic processes I: General model and Energy-Constrained Assimilation and Fractional Crystallization (EC-AFC) formulation. *Journal of Petrology*, *42*(5), 999–1018.
Sun, S. S., & McDonough, W. F. (1989). Chemical and isotopic systematics of oceanic basalts: Implications for mantle composition and processes. In A. D. Saunders & M. J. Norry (Eds.), *Magmatism in the ocean basins* (pp. 313–345). London, UK: Geological Society.
Tang, G.-J., Chung, S.-L., Wang, Q., Wyman, D. A., Dan, W., Chen, H.-Y., & Zhao, Z.-H. (2014). Petrogenesis of a Late Carboniferous mafic dike–granitoid association in the western Tianshan: Response to the geodynamics of oceanic subduction. *Lithos*, *202–203*, 85–99.
Tang, G.-J., Chung, S.-L., Hawkesworth, C. J., Cawood, P. A., Wang, Q., Wyman, D. A., . . . Zhao, Z.-H. (2017a). Short episodes of crust generation during protracted accretionary processes: Evidence from Central Asian Orogenic Belt, NW China. *Earth and Planetary Science Letters*, *464*, 142–154.
Tang, G.-J., Wang, Q., Wyman, D. A., Chung, S.-L., Chen, H.-Y., & Zhao, Z.-H. (2017b). Genesis of pristine adakitic magmas by lower crustal melting: A perspective from amphibole composition. *Journal of Geophysical Research: Solid Earth*, *122*, 1934–1948. https://doi.org/10.1002/2016JB013678
Tang, G. J., Wang, Q., Wyman, D., Sun, A. M., Li, Z. X., Zhao, Z. H., . . . Jiang, Z. Q. (2010). Geochronology and geochemistry of Late Paleozoic magmatic rocks in the Lamasu–Dabate area, northwestern Tianshan (west China): Evidence for a tectonic transition from arc to post-collisional setting. *Lithos*, *119*(3–4), 393–411.
Tatsumi, Y., Hamilton, D. L., & Nesbitt, R. W. (1986). Chemical characteristics of fluid phase released from a subducted lithosphere and origin of arc magmas: Evidence from high-pressure experiments and natural rocks. *Journal of Volcanology and Geothermal Research*, *29*(1–4), 293–309.
Turner, S., Arnaud, N., Liu, J., Rogers, N., Hawkesworth, C., Harris, N., . . . Deng, W. (1996). Post-collision, shoshonitic volcanism on the Tibetan Plateau: Implications for convective thinning of the lithosphere and the source of ocean island basalts. *Journal of Petrology*, *37*(1), 45–71.
von Blanckenburg, F., & Davies, J. H. (1995). Slab breakoff: A model for syncollisional magmatism and tectonics in the Alps. *Tectonics*, *14*(1), 120–131.
von Huene, R., & Scholl, D. W. (1991). Observations at convergent margins concerning sediment subduction, subduction erosion, and the growth of continental crust. *Reviews of Geophysics*, *29*(3), 279–316.
Wiedenbeck, M., AllÉ, P., Corfu, F., Griffin, W., Meier, M., Oberli, F., . . . Spiegel, W. (1995). Three natural zircon standards for U–Th–Pb, Lu–Hf, trace element and REE analyses. *Geostandard. Newslett*, *19*(1), 1–23.
Williams, H. M., Turner, S. P., Pearce, J. A., Kelley, S. P., & Harris, N. B. W. (2004). Nature of the source regions for post-collisional, potassic magmatism in southern and northern Tibet from geochemical variations and inverse trace element modelling. *Journal of Petrology*, *45*(3), 555–607.
Woodhead, J., Hergt, J., Greig, A., & Edwards, L. (2011). Subduction zone Hf-anomalies: Mantle messenger, melting artefact or crustal process? *Earth and Planetary Science Letters*, *304*(1–2), 231–239.
Wu, C.-Z., Zhang, Z.-Z., Gu, L.-X., Tang, J.-H., & Lei, R.-X. (2010). Sr, Nd and O isotopic characters of quartz syenite in the Weiya magmatic complex from eastern Tianshan in NW China: Melting of the thickened juvenile lower crust. *Geochemical Journal*, *44*(4), 285–298.
Wu, F. Y., Yang, Y. H., Xie, L. W., Yang, J. H., & Xu, P. (2006). Hf isotopic compositions of the standard zircons and baddeleyites used in U-Pb geochronology. *Chemical Geology*, *234*(1–2), 105–126.
Wyman, D. A., & Kerrich, R. (1993). Archean Shoshonitic Lamprophyres of the Abitibi Subprovince, Canada: Petrogenesis, Age, and Tectonic Setting. *Journal of Petrology*, *34*(6), 1067–1109.
Xiao, W., Windley, B. F., Allen, M. B., & Han, C. (2013). Paleozoic multiple accretionary and collisional tectonics of the Chinese Tianshan orogenic collage. *Gondwana Research*, *23*(4), 1316–1341.
Xu, X. Y., Xia, L. Q., Ma, Z. P., Wang, Y. B., Xia, Z. C., Li, X. M., & Wang, L. S. (2006). SHRIMP zircon U-Pb geochronology of the plagiogranites from Bayringou ophiolite in North Tianshan Mountains and the petrogenesis of the ophiolite [in Chinese with English abstract]. *Acta Petrologica Sinica*, *22*(1), 83–94.
Yan, S., Shan, Q., Niu, H.-C., Yang, W.-B., Li, N.-B., Zeng, L.-J., & Jiang, Y.-H. (2015). Petrology and geochemistry of late Carboniferous hornblende gabbro from the Awulale Mountains, western Tianshan (NW China): Implication for an arc–nascent back-arc environment. *Journal of Asian Earth Sciences*, *113*, 218–237.
Yang, J. H., Sun, J. F., Chen, F. K., Wilde, S. A., & Wu, F. Y. (2007). Sources and petrogenesis of late Triassic dolerite dikes in the Liaodong Peninsula: Implications for post-collisional lithosphere thinning of the eastern north China craton. *Journal of Petrology*, *48*(10), 1973–1997.
Ye, H., Ye, X., & Zhang, C. (2013). Geochemistry and geodynamic implications of Nileke Permian volcanic rocks in Western Tianshan, NW China. *Acta Petrologica Sinica*, *29*(10), 3389–3401.
Yuan, C., Sun, M., Wilde, S., Xiao, W., Xu, Y., Long, X., & Zhao, G. (2010). Post-collisional plutons in the Balikun area, East Chinese Tianshan: Evolving magmatism in response to extension and slab break-off. *Lithos*, *119*(3–4), 269–288.
Zhao, Z., Mo, X., Dilek, Y., Niu, Y., DePaolo, D. J., Robinson, P., . . . Hou, Z. (2009). Geochemical and Sr–Nd–Pb–O isotopic compositions of the post-collisional ultrapotassic magmatism in SW Tibet: Petrogenesis and implications for India intra-continental subduction beneath southern Tibet. *Lithos*, *113*(1–2), 190–212.
Zhao, Z. H., Xiong, X. L., Wang, Q., Wyman, D. A., Bao, Z. W., Bai, Z. H., & Qiao, Y. L. (2008). Underplating-related adakites in Xinjiang Tianshan, China. *Lithos*, *102*(1–2), 374–391.